2D Phase Purity Determines Charge Transfer Yield at 3D/2D Lead Halide Perovskite Heterojunctions

Robert J. E. Westbrook[1,2,3]*, Weidong Xu[1,3], Xinxing Liang[1,3], Thomas Webb,[4] Tracey M. Clarke[2], Saif A. Haque[1,3]*

[1]Department of Chemistry, Imperial College London, Molecular Sciences Research Hub

White City Campus, Wood Lane, W12 0BZ, UK

[2]Department of Chemistry, University College London, 20 Gordon Street, London WC1H 0AJ, UK

[3]Centre for Processable Electronics, Imperial College London, London SW7 2AZ, UK

[4]Advanced Technology Institute, Department of Electrical and Electronic Engineering, University of Surrey, Guildford, Surrey, GU2 7XH, UK

*__Corresponding Authors__: R.J.E.W (r.westbrook15@imperial.ac.uk); S.A.H (s.a.haque@imperial.ac.uk)

Abstract:

Targeted functionalisation of 3D perovskite with a 2D passivation layer via R-NH_3I treatment has emerged as an effective strategy for enhancing both the efficiency and chemical stability of ABX_3 perovskite solar cells, but the underlying mechanisms behind these improvements remain unclear. Here, we assign a passivation mechanism where R-NH_3I reacts with excess PbI_2 in the $MAPbI_3$ film and unsaturated PbI_6 octahedra to form $(R\text{-}NH_3)_2(MA)_{1\text{-}n}Pb_nI_{3n+1}$. Crucially, we show that precise control of the 2D $(R\text{-}NH_3)_2(MA)_{1\text{-}n}Pb_nI_{3n+1}$ layer underpins performance improvements: n = 1 yields over a two-fold improvement in hole injection to the HTL; n > 1 deteriorates hole injection. Ultrafast transient absorption spectroscopy suggests this n-dependence is rooted in the fact that fast (< 6ns) hole injection does not occur between the 3D and 2D layers. These results help explain contemporary empirical findings in the field and set out an important design rule for the further optimisation of multidimensional perovskite optoelectronics.

TOC:

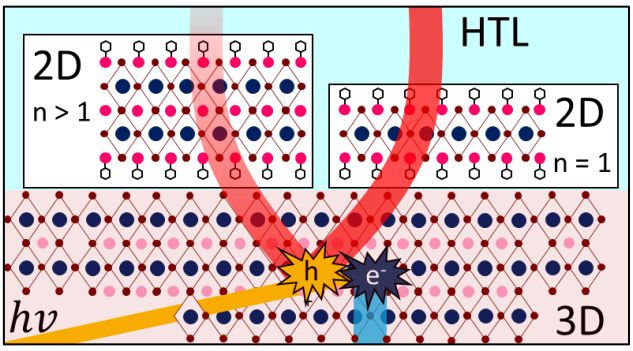

An intense research effort over the last decade has driven the meteoric rise in power conversion efficiency (PCE) of perovskite solar cells (PSCs) to values over 25%.[1] Today, many of their remaining short-comings can be traced back to structural defects. Remarkably, harmful bulk defects that form electronic states within the band-gap – i.e. traps – are found at relatively low concentrations in hybrid perovskites compared to other solution processed technologies.[2] However, the interruption of crystal symmetry at the surface and grain boundaries inevitably leads to a significant population of traps at the interfaces with the charge transport layers (CTLs).[3–5] Such trap-states ultimately limit the quasi-Fermi level splitting (QFLS) of electrons and holes under illumination, and thus the open-circuit voltage (V_{OC}), in $MAPbI_3$ to below the theoretical maximum of 1.32 V,[6] and lead to current voltage hysteresis and chemical instability.[7–9]

Braly *et al* showed that Lewis base passivation of positively charged traps in $MAPbI_3$ such as iodide vacancies (V_I) with electron donating tri-*n*-octylphosphide (TOPO) leads to an internal QFLS of 1.28 eV.[10] The implication of this is that the bulk material does not intrinsically limit the V_{OC} and that effective trap passivation at the surface and grain boundaries should lead to values approaching the radiative limit. Therefore, an intense research effort has set about developing strategies that emulate such passivation with other small molecules, inert polymers and CTLs.[11–18]

Treatment of perovskite with iodide salts is another well-established passivation strategy. It has been shown that adding over-stoichiometric (< 5 wt%) amounts of small iodide salts - where 'small' is here defined as those salts containing an $R\text{-}NH_3^+$ cation that would satisfy Goldschmidt's tolerance factor if incorporated into a traditional 3D perovskite lattice[19] - to the perovskite precursor mixture can yield devices with a slightly larger PCE, but when applied in excess, the build-up of unreacted $R\text{-}NH_3I$ can degrade device performance.[20–22] On the other hand, introducing 2D character to perovskite by adding bulky ammonium iodide salts ($R\text{-}NH_3I$) – i.e. those that cannot be incorporated into the 3D perovskite lattice – has come to the fore as an effective passivation strategy. The $R\text{-}NH_3I$ is either added to the precursor solution to induce bulk passivation[23,24] or as a post-treatment to

provide targeted functionalisation of the perovskite|CTL interface [where CTL = hole transport layer (HTL) in *nip*, electron transport layer (ETL) in *pin*].[25–27] In the latter strategy, a layer of reduced-dimensional perovskite (RDP) with formula $(R\text{-}NH_3)_2(MA)_{1\text{-}n}Pb_nI_{3n+1}$ is formed between the 3D perovskite layer and the CTL. Such 3D/RDP PSCs have superior stability than their purely 3D counterparts,[24,28–30] which is often attributed to the hydrophobicity of the $R\text{-}NH_3^+$ ions in the RDP layer.[31–33]

Less clear is the role of the RDP layer in enhancing charge extraction and ultimately device PCE.[26,28–30,33–35] Here, the progression of research has largely relied on empirical observations, rather than rigid design rules based on a comprehensive understanding of the 3D/RDP system. Pioneering work has elucidated the importance of energy cascades, energy transfer and charge mobility in the 3D/RDP system,[36–39] but a consistent model for hole injection at the 3D/RDP|HTL interface is still lacking. The Grancini group has made significant steps forward in this regard, showing that effective RDP-on-3D passivation is predicated by a flat conformation of the RDP layer.[40] In another study, they showed that the 3D/RDP interface is dynamic, in that the RDP layer - initially consisting largely of $(R\text{-}NH_3)_2PbI_4$ (n = 1) - can scavenge intrinsic MA cations from the 3D perovskite to form device-limiting, higher order $(R\text{-}NH_3)_2(MA)_{n\text{-}1}Pb_nI_{3n+1}$ (n = 1, 2…) heterostructures, which can be proscribed by careful design of the RDP-inducing passivant.[41] Elsewhere, Teale *et al* developed a technique for dimensional mixing of the passivating RDP layer. They used grazing incidence wide-angle X-ray scattering (GIWAXS) to suggest that device PCE was enhanced for mixed-n RDPs, but suggested that further study should be carried out with more precise optical techniques.[42] Interestingly, the common denominator in the latter two studies is the significance of the n value in the passivating $(R\text{-}NH_3)_2(MA)_{1\text{-}n}Pb_nI_{3n+1}$ layer. However, the link between the value of n and charge extraction remains unseen. Additionally, it is unclear whether the RDP layer actively mediates hole injection in 3D/RDP|HTL systems,[26,43,44] or forms an electronically benign passivating layer.[23,40]

Herein, we use a combination of surface sensitive structural and time-resolved optical spectroscopy to elucidate the full scale of passivation in n-i-p $MAPbI_3$ perovskite films treated with R-NH_3I salts. We show that bulkiness is a prerequisite to enhancements in the injection efficiency, with smaller cations actually working to reduce charge extraction by forming trapping centres. We reveal that the improvements with bulky cations are due to the treatment of excess PbI_2 with R-NH_3I to form (R-$NH_3)_2(MA)_{n-1}Pb_nI_{3n+1}$ at the $MAPbI_3$|HTL interface. Moreover, we gain new insights into the charge separation mechanism at the $MAPbI_3$|(R-$NH_3)_2(MA)_{n-1}Pb_nI_{3n+1}$|HTL (3D/RDP|HTL) interface: (i) the RDP layer does not mediate hole injection between the 3D perovskite and HTL; (ii) efficient hole injection is only possible for n = 1 and is significantly inhibited in systems where n > 1. These results yield an important design rule for the development of high performance 3D/2D perovskite optoelectronics.

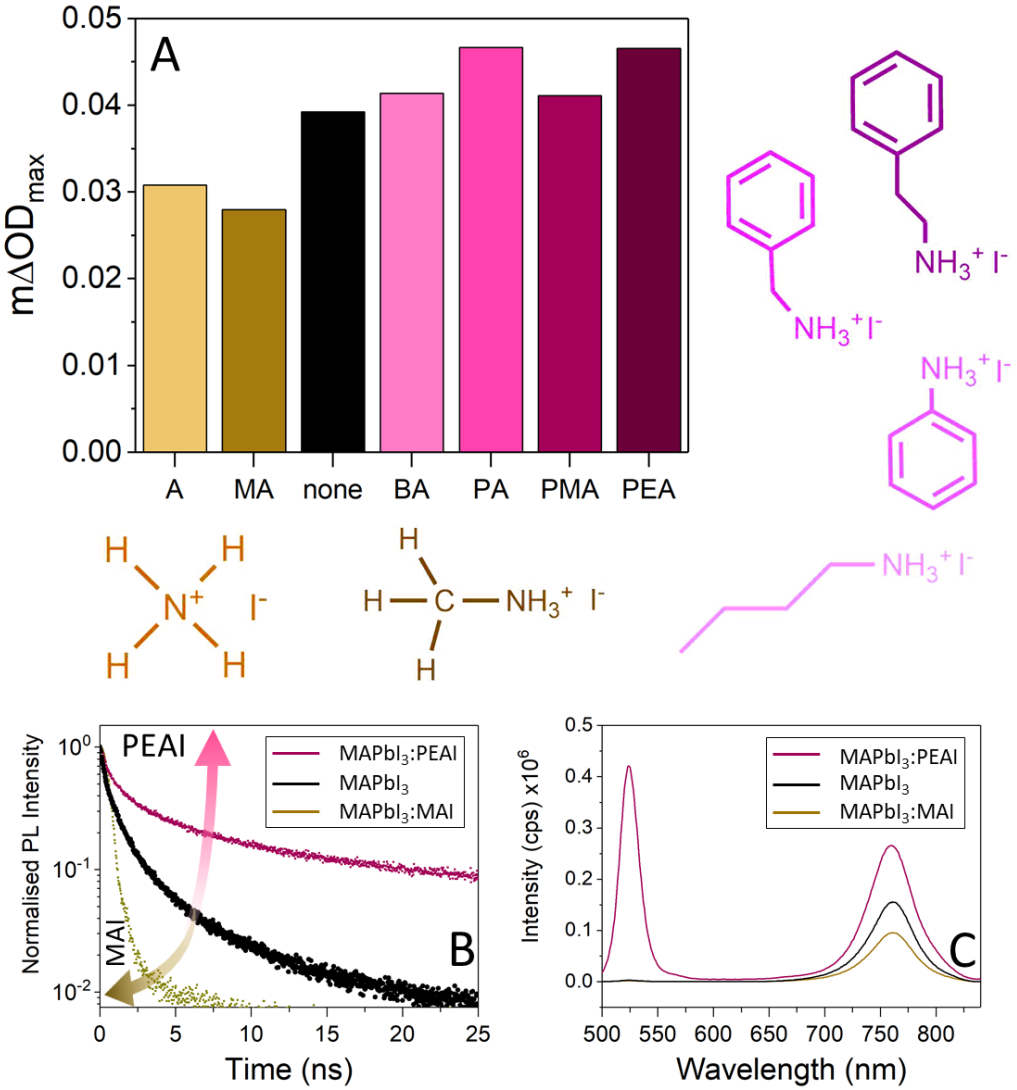

Figure 1. (a) ΔOD_{max} - i.e. ΔOD from transient absorption spectroscopy (TAS) measured 1 µs after excitation - for TiO_2|$MAPbI_3$:R-NH_3I (20 mM)|PTAA samples, where R-NH_3^+ is ammonium (A), methylammonium (MA), butylammonium (BA), phenylammonium (PA), phenylmethylammonium (PMA) and phenethylammonium (PEA). The same parameter for a $MAPbI_3$|HTL sample with no passivation treatment is given in black. The samples were excited at a wavelength of 510 nm and pulse fluence of 10 µJ cm^{-2}. A probe wavelength of 1500 nm was used to identify injected holes in the HTL layer. The structures of the passivating agents surround (a); anti-clockwise: AI, MAI, BAI, PAI, PMAI and PEAI. (b) Time-resolved single photon counting (TCSPC) decays of $MAPbI_3$ films treated with 20 mM PEAI (magenta) and MAI (brown). The control $MAPbI_3$ decay with no coating is given in black. Samples were excited with a pump wavelength of 635 nm at 0.11 nJ cm^{-2} and probed at 760 nm. (c) Steady-state photoluminescence of the samples after excitation via the film surface with a wavelength of 450 nm at 260 mW cm^{-2}.

In order to investigate the role of chemical structure in determining the efficacy of passivation, we screened methylammonium and phenethylammonium (MAI and PEAI) and several other R-NH_3I (R = ammonium, phenylammonium, phenylmethylammonium, butylammonium) salts. We note that

samples were prepared via a one-step deposition of $MAPbI_3$ with a 1:1 PbI_2:MAI ratio as reported elsewhere,[45] followed by iodide salt treatment and annealing as outlined in the supporting information.

Device efficiency is ultimately based on the yield of sustained charge injection at the interfaces between $MAPbI_3$ and its CTLs. Therefore, we first investigated the role of the R-NH_3I cation in determining the hole transfer yield at the $MAPbI_3$:R-NH_3I|HTL interface with microsecond transient absorption spectroscopy (µs-TAS). Details of the µs-TAS technique and set-up can be found in the supporting information. Figure S1 shows that $MAPbI_3$ exhibits no transient absorption features on the microsecond timescale, which is in line with the typical 10-100 ns recombination timescale for this material in the fluence range used. On the other hand, when interfaced with the HTL poly-(triarylamine) (PTAA), a broad TA feature is observed with a maximum signal strength, ΔOD_{max} at 1500 nm, which can be attributed to hole polarons in PTAA formed after injection from the $MAPbI_3$ valence band.[46,47] Given the proportionality between ΔOD_{max} and the concentration of injected holes in PTAA, we could then track the impact of each R-NH_3I treatment on hole transfer to the HTL.

Figure 1 shows the relative hole injection yield (i.e. ΔOD_{max}) in $MAPbI_3$|HTL films in the case of passivation with 20mM of the different iodide salts. Strikingly, only the iodide salts with bulky cations i.e. those to the right of the control (black) film in Figure 1 can improve the hole injection yield to the HTL.

In contrast, application of MAI and AI to $MAPbI_3$ results in a reduction in hole injection yield at the $MAPbI_3$|HTL interface. This supports work elsewhere in the literature, where MAI applied in great excess, or as a post-treatment, works to lower the PCE of PSCs.[20–22] In order to understand this surprising result, we turned to steady-state and time-resolved photoluminescence (PL) spectroscopy using MAI as an example salt treatment with a small cation. In Figure 1b and c we see that the lifetime and intensity of the $MAPbI_3$ film after MAI treatment are much reduced. This suggests that

the addition of MAI adds additional trap-states through which the photoexcited charges in the $MAPbI_3$ layer can recombine.

Consideration of the reaction between MAI and the perovskite film leads to a potential explanation for the increase in trap density after MAI passivation and annealing. As-crystallised $MAPbI_3$ contains an excess of PbI_2 at the grain boundaries due to the ready escape of MAI during annealing.[48] This excess PbI_2 is known to improve the performance of perovskite solar cells through a passivation effect,[48–50] and may also lower the hole injection barrier at the $MAPbI_3$|HTL interface, improving hole extraction.[49,50] We display evidence for the formation of excess PbI_2 with grazing-incidence X-ray diffraction (GIXRD) measurements in Figure S2, where our control $MAPbI_3$ film shows a peak at 2θ = 12.6° associated with the (001) orientation of unreacted PbI_2.[51] We also observe a contribution at 2θ = 14.2°, associated with the (110) orientation of the 3D perovskite. The removal of the 2θ = 12.6° peak in the MAI-treated sample (Figure S2, second panel) suggests that the MAI reacts with PbI_2, removing its beneficial passivation effects. We note that the peak position of the (110) contribution associated with 3D perovskite remains unchanged and the intensity is not reduced, allowing us to discard the idea that MAI treatment deteriorates performance by exerting strain on, or damaging, the pre-existing 3D perovskite structure.[52]

On the other hand, $MAPbI_3$ films treated with R-NH_3I salts containing bulky R-NH_3^+ cations consistently exhibit greater hole injection yields than the unpassivated control. The enhanced PL lifetime and intensity in $MAPbI_3$:PEAI films exhibited in Figure 1b and c provides strong evidence that recombination of photoexcited charge carriers in $MAPbI_3$ is much supressed after PEAI treatment. Furthermore, the entirely opposite effect of PEAI compared to MAI treatment on charge separation in the $MAPbI_3$ film suggests that the cation plays a decidedly different role in the former case. Further insight into the mechanism of passivation in the case of $MAPbI_3$:PEAI films is given in Figure 1c, where an additional PL contribution can be observed at 525 nm.

As has been established elsewhere,[26,35] passivation with bulky organic cations leads to the formation of a reduced dimensional perovskite (RDP) layer with formula $(PEA)_2(MA)_{1-n}Pb_nI_{3n+1}$ at the top surface of the 3D perovskite film due to the inability of the cation to intercalate into a traditional 3D perovskite lattice. We therefore attribute the 525 nm feature to $(PEA)_2PbI_4$ atop the 3D perovskite film. We provide further evidence for this in Figure S3, where we excited 3D/RDP at 450 nm (penetration depth ~ 100 nm) from the film and substrate faces of the film respectively and measured the PL. The much enhanced intensity of the 525 nm contribution after excitation from the film face confirms that the RDP layer is concentrated at the top surface of the $MAPbI_3$ film.

Moreover, in Figure S4 we present the PL spectra of 3D perovskite treated with the other bulky R-NH_3I salts (i.e. PAI, PMAI, BAI). The features observed in the 500-550 nm region of the spectrum indicate the formation of $(R\text{-}NH_3)_2(MA)_{n-1}Pb_nI_{3n+1}$ heterostructures in all cases. This is in good agreement with the literature, where bulky R-NH_3I salts such as these are routinely used to induce RDP layers.[25,28,53] We can therefore conclude that bulky R-NH_3^+ cations are prerequisite to the enhancements in interfacial charge injection observed after iodide salt passivation.

We also carried out GIXRD to obtain interface specific insight into the formation of the RDP (Figure S2). Notably, in the case of passivation with the R-NH_3I salts, the (001) peak associated with PbI_2 is entirely removed after all but PAI treatment, which still shows a substantial reduction in intensity. This suggests that the RDP layers are seeded by reaction between R-NH_3I and excess PbI_2 at the 3D perovskite surface.

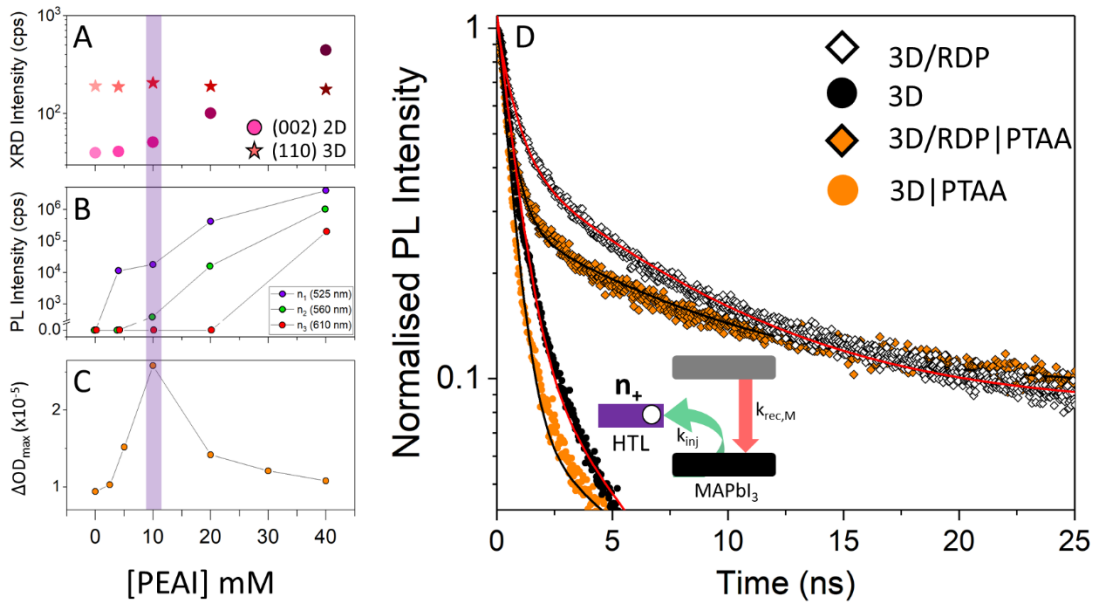

Figure 2. Hole injection in 3D/RDP|HTL films. (a) Change in the (110) peak from 3D perovskite (☆) and the (002) peak from the RDP passivating layer (●) with [PEAI]. (b) Evolution of the RDP photoluminescence spectrum in 3D/RDP films at 525 (n = 1; purple), 560 (n = 2; green) and 610 nm (n = 3, red) respectively as a function of [PEAI]. (c) ΔOD_{max} – i.e. ΔOD from transient absorption spectroscopy (TAS) measured 1 µs after excitation - of 3D/RDP|PTAA films with increasing [PEAI]. The films were excited at 510 nm (fluence: 1.5 µJ cm^{-2}) and probed at 1500 nm, the maximum of the PTAA polaron. (d) Time-resolved single photon counting (TCSPC) decays for 3D (solid points) and 3D/RDP films (empty points) with and without PTAA (orange) (excitation: 635nm; fluence of 0.11 nJ cm^{-2}; probe: 760 nm).

Table 1. Biexponential fitting ($y(t) = A_1e^{-t/\tau_1} + A_2e^{-t/\tau_2}$) parameters for the time-resolved single photon counting (TCSPC) decays given in Figure 2. We note that $\tau_1 = \tau_{inj}$ for PTAA-coated samples.

Sample	A_1	$\tau_1 (= \tau_{inj})$ (ps)	A_2	τ_2 (ps)
3D	0.928	**669**	0.0716	4500
3D/RDP	0.672	**708**	0.328	6700
3D|PTAA	0.993	**503**	0.0823	4716
3D/RDP|PTAA	0.772	**513**	0.194	7450

We next looked to quantify exactly how interfacial hole injection correlates with the growth of the RDP passivating layer on the 3D perovskite by increasing the concentration of PEAI from 4 mM to 40 mM. Given the potential for PEA^+ to combine with intrinsic MA^+ from the 3D perovskite film to form $(PEA)_2(MA)_{n-1}Pb_nI_{3n+1}$, we paid particular attention to the formation of n > 1 RDP layers.

We first investigated the growth of the RDP on 3D perovskite as a function of [PEAI] with XRD. Raw XRD patterns (Figure S5) exhibit strong diffraction peaks for 3D perovskite films at 14.2, 28.5 and 32.5°, which are associated with the (110), (220) and (310) lattice orientations of 3D tetragonal

halide perovskite.[48] Furthermore, the (002) orientation of $(PEA)_2PbI_4$, present within the RDP becomes increasingly prevalent as a function of [PEAI].[26] In Figure 2a we track the evolution of the (110) and (002) characteristic peaks of the 3D perovskite and RDP respectively as a function of [PEAI]. This data suggests that the RDP is present even at a relatively low concentration of 10 mM. Moreover, for [PEAI] > 10 mM, the 3D perovskite contribution reduces in intensity, suggesting significant damage to the underlying 3D perovskite layer at high PEAI concentrations.

We next turned to PL spectroscopy hoping that the orders of magnitude greater sensitivity of this technique could reveal more about the 2D character of the passivated films. In Figure 2b we summarise the evolution of the RDP with [PEAI] by tracking the $(PEA)_2PbI_4$ (n = 1), $(PEA)_2(MA)Pb_2I_7$ (n = 2) and $(PEA)_2(MA)_2Pb_3I_{10}$ (n = 3) contributions in the PL spectra at 525, 560 and 610 nm respectively (raw spectra in Figure S6).[41,54,55] Interestingly, we find that the n > 1 features for the [PEAI] $\leq$ 10 mM samples are minimal when compared to the n = 1 contribution. Notably, the contribution from the n = 2 structure increases with [PEAI] thereafter to 4% and 25% for 20 mM and 40 mM respectively. Additionally, a third contribution associated with the n = 3 structure is present at 5% in the PL spectrum of the 40 mM film. It can therefore be concluded that an almost phase pure $(PEA)_2PbI_4$ layer is formed after PEAI treatment at concentrations equal to or below 10 mM due to the consumption of the excess PbI_2 in the film. At higher concentrations, we suggest that the additional PEAI begins to attack the perovskite itself - presumably at unsaturated PbI_6 octahedra via V_{MA} sites - and combines with intrinsic MA^+ to form higher order RDP (n > 1) heterostructures.

We next assessed the impact of RDP growth on the relative hole injection yield i.e. ΔOD_{max} from µs-TAS. The results in Figure 2c show that the relationship between hole injection and [PEAI] is non-trivial, reaching a maximum at 10 mM. Importantly, this is the concentration at which the largest amount of phase-pure $(PEA)_2PbI_4$ (i.e. n = 1) RDP is formed, with minimal formation of higher-order n > 1 structures. Indeed, the formation of these higher order structures in the passivating layer is concomitant with a decrease in the hole injection yield.

To probe the origin of this maximum in hole injection yield at 10 mM, we captured PL decay dynamics for 3D|HTL and 3D/RDP|HTL with the results displayed in Figure 2d. The PL decay of 3D perovskite can be fitted to a biexponential with a fast (τ_1) and slow (τ_2) component indicative of charge trapping at grain boundaries and in the bulk respectively.[56] Upon addition of a HTL, the fast decay ($\tau_1 = \tau_{inj}$) becomes indicative of hole injection and the slow component (τ_2) is due to either unquenched charges that remain in the bulk,[57] or surface recombination.[5] The rapid (τ_{inj} = 503 ps) hole injection kinetics observed after interfacing 3D perovskite with PTAA are in line with previous literature reports,[46] attributed to the significant energetic offset ($\Delta E \sim$ 0.2 eV) at the 3D|PTAA interface. We note that τ_{inj} here is much larger than the instrumental response of our TCSPC set-up ($\tau_{IRF} \sim$ 100 ps) allowing for accurate assignation of these kinetics. Importantly, τ_{inj} (=513 ps) for 3D/RDP|PTAA is similar to 3D|PTAA (Table 1, bold), suggesting that the RDP layer has little impact on the kinetics of hole injection at the 3D/RDP|HTL interface. In light of this, we rationalise the increased hole injection yield (n_+ in Figure 2d: inset) at [PEAI] = 10 mM as a decrease of the recombination rate constant in the 3D layer ($k_{rec,M}$), rather than an increase in the hole injection rate constant (k_{inj}).

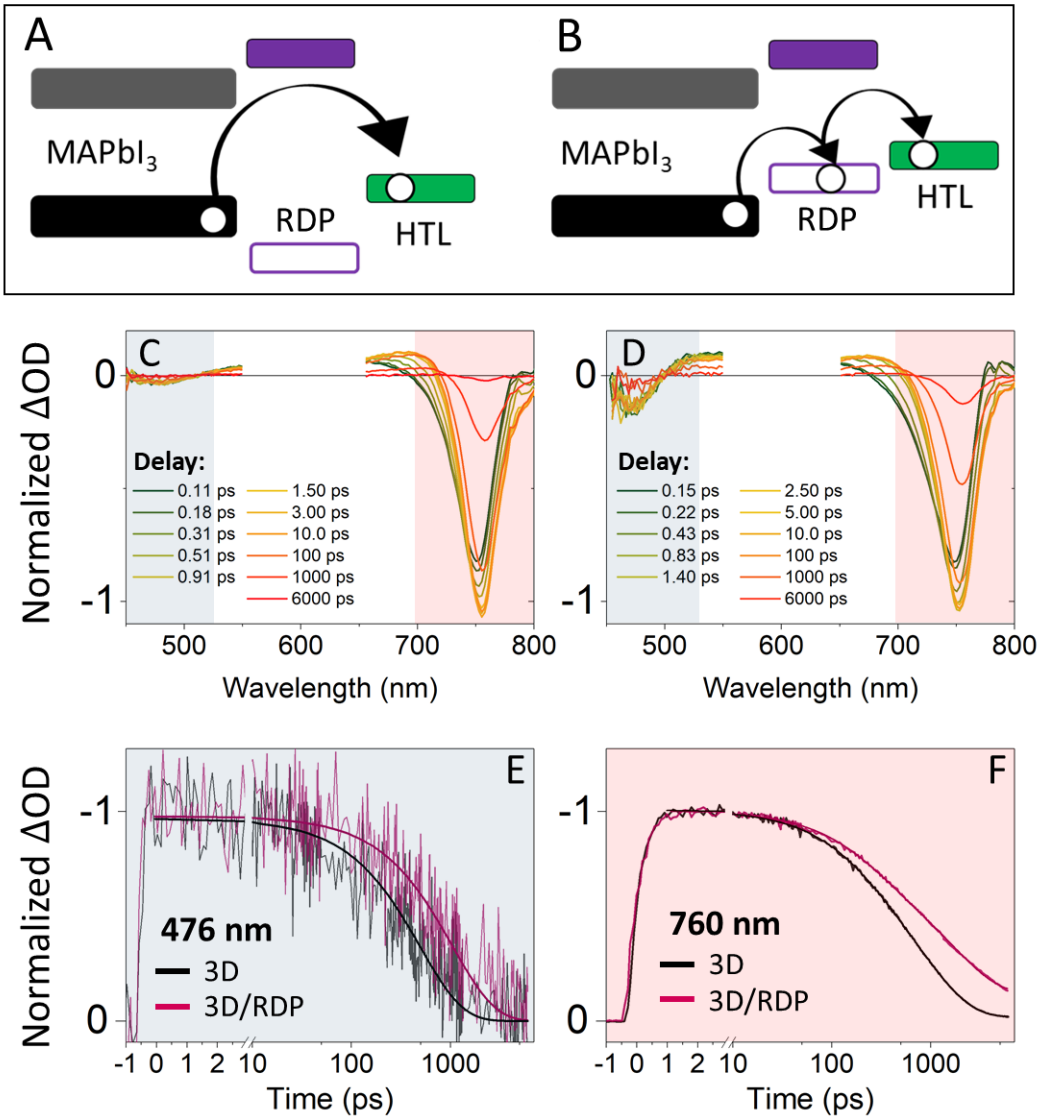

Figure 3. Charge Injection Mechanism in 3D/RDP|HTL formed after treating $MAPbI_3$ with 10 mM PEAI. Illustration of the two possible mechanisms for hole injection at the 3D/RDP|HTL interface: (a) tunnelling injection (type I interface) and (b) mediated hole injection (type II interface). Femtosecond transient absorption spectra of (c) 3D and (d) 3D/RDP films as a function of time. The two key photoinduced absorption features at 476 nm (blue) and 760 nm (red) are highlighted. The decay dynamics in the case of 3D (black) and 3D/RDP (pink) at 476 nm and 760 nm are shown in (e) and (f) respectively. Films were pumped at 635 nm (fluence: 25 μJ cm^{-2}), resulting in the 550-650 nm gap in the spectra.

The findings presented so far prove that upon passivation of 3D perovskite with 10 mM PEAI: (i) an almost phase-pure $(PEA)_2PbI_4$ layer is formed; (ii) this layer is positioned at the 3D|HTL interface; and (iii) hole injection is not impeded by the $(PEA)_2PbI_4$ passivating layer. We therefore next looked to build a picture of the interfacial energetics to explain these observations.

While it is established that the conduction band minimum (CBM) of RDPs lie well above the CBM of $MAPbI_3$,[23,40,43,58–60] reporting on the position of the valence band maximum (VBM) has not been consistent. This is most likely due to variations in band-gap (n value) and ligand coverage, both of which have a significant impact on the VBM.[42] Cho *et al* reported that the valence band (VB) energy of $(PEA)_2PbI_4$ is similar to that in $MAPbI_3$.[26] In contrast, several other literature reports place the VBM of RDPs as shallower than the 3D VBM.[43,44] Elsewhere, another group of reports place the VBM of RDPs as deeper than the 3D VBM.[23,40,58] As such, depending on the literature report, the 3D/RDP interface alternates between type I (3D band-gap lies within the RDP band-gap) and type II (only the 3D conduction band lies within the RDP band-gap), which has important implications for the mechanism of hole injection at the 3D/RDP|HTL interface. In the type I case, the RDP VB lies below that of $MAPbI_3$ and hole injection to the HTL occurs via tunnelling (Figure 3a). Otherwise, in the type II case, the RDP VB lies between that of $MAPbI_3$ and the HTL HOMO, and thus mediates hole injection (Figure 3b).

In order to establish which of the two proposed mechanisms is at work, we conducted femtosecond-TAS (fs-TAS) studies on 3D and 3D/RDP films formed after treatment of 3D perovskite with the optimised concentration of 10 mM PEAI. We probed the visible/near infra-red (400-800 nm) region after exciting the samples at 635nm and found two distinct bleaching peaks at ~476 nm (PB1) and ~760 nm (PB2). PB2 is assigned to the band edge transition of 3D perovskite, which is in line with the absorption onset of the 3D perovskite film in Figure S7 at 760 nm. The origin of PB1 is debated but may be due either to excitation from a deeper valence band,[61,62] or a charge transfer state involving PbI_x^- complexes.[63] The broad positive band between 500-700 nm is assigned to photoinduced absorption (PIA), potentially from I_2-like reversable photo-dissociation products of PbI_x^-.[63]

As indicated in Figure S7, 2D $(PEA)_2PbI_4$ has a strong ground-state absorption beginning at 525 nm. In TA spectra, this absorption can lead to a photobleaching feature (PB3) between 500 and 525 nm.[36,40]

We hypothesised that if the $(PEA)_2PbI_4$ layer plays an active role in mediating hole injection, PB3 would be present in the TA spectrum at time τ_{inj} after initial excitation of the 3D perovskite. However, the shape of the 3D (Figure 3c) and 3D/RDP (Figure 3d) spectra are strikingly similar across the 6 ns time window for the measurement. This result suggests that no hole injection occurs between the 3D perovskite and RDP layer.

We note that the RDP layer in the optimised system – after treatment with 10 mM PEAI – is very thin, and so PB3 (maximum $\sim$ 500 nm) could be buried by PB1 (maximum $\sim$ 476 nm), which is assigned to the much thicker 3D perovskite film. However, we show in Figure S8 that even for a much thicker RDP layer – after 40 mM PEAI treatment – still no features are observed that can be attributed to PB3. This adds weight to our argument that no injection occurs between the 3D and RDP layers.

In agreement with our time-resolved PL studies we find an increased lifetime of photoexcited charges in the 3D/RDP samples (Figure 3e and f, magenta lines) compared to pure 3D (Figure 3e and f, black lines). Additionally, we checked the decay of PB1 and PB2 for signs of 3D to RDP injection. This would be evidenced by a rising component in PB1 – due to proximity to the RDP GSB - and a 'quenching' component in PB2 – due to depopulation of the 3D perovskite after injection to the RDP. However, no such abnormalities in the recombination kinetics were observed.

Combining this with the lack of new features associated with PB3 in the 3D/RDP TA spectra, we suggest that the $(PEA)_2PbI_4$ layer formed after PEAI passivation does not accept holes from the 3D perovskite on the timescales studied (< 6 ns). Given that hole injection to the HTL in the best-performing PSC devices occurs on faster timescales – often sub-nanosecond as observed in Figure 2d and elsewhere[46,64] – we can say with some certainty that the $(PEA)_2PbI_4$ layer in our 3D/RDP system does not actively mediate hole injection. This suggests that the 3D/RDP interface is type I, as put forward elsewhere.[23,40,58] Given RDP coverage on the 3D perovskite surface is likely incomplete in the optimised system, hole injection can occur via two potential mechanisms: (i) tunnelling at the

3D/RDP|HTL interface; and (ii) direct injection in regions of immediate contact between the 3D perovskite and HTL.

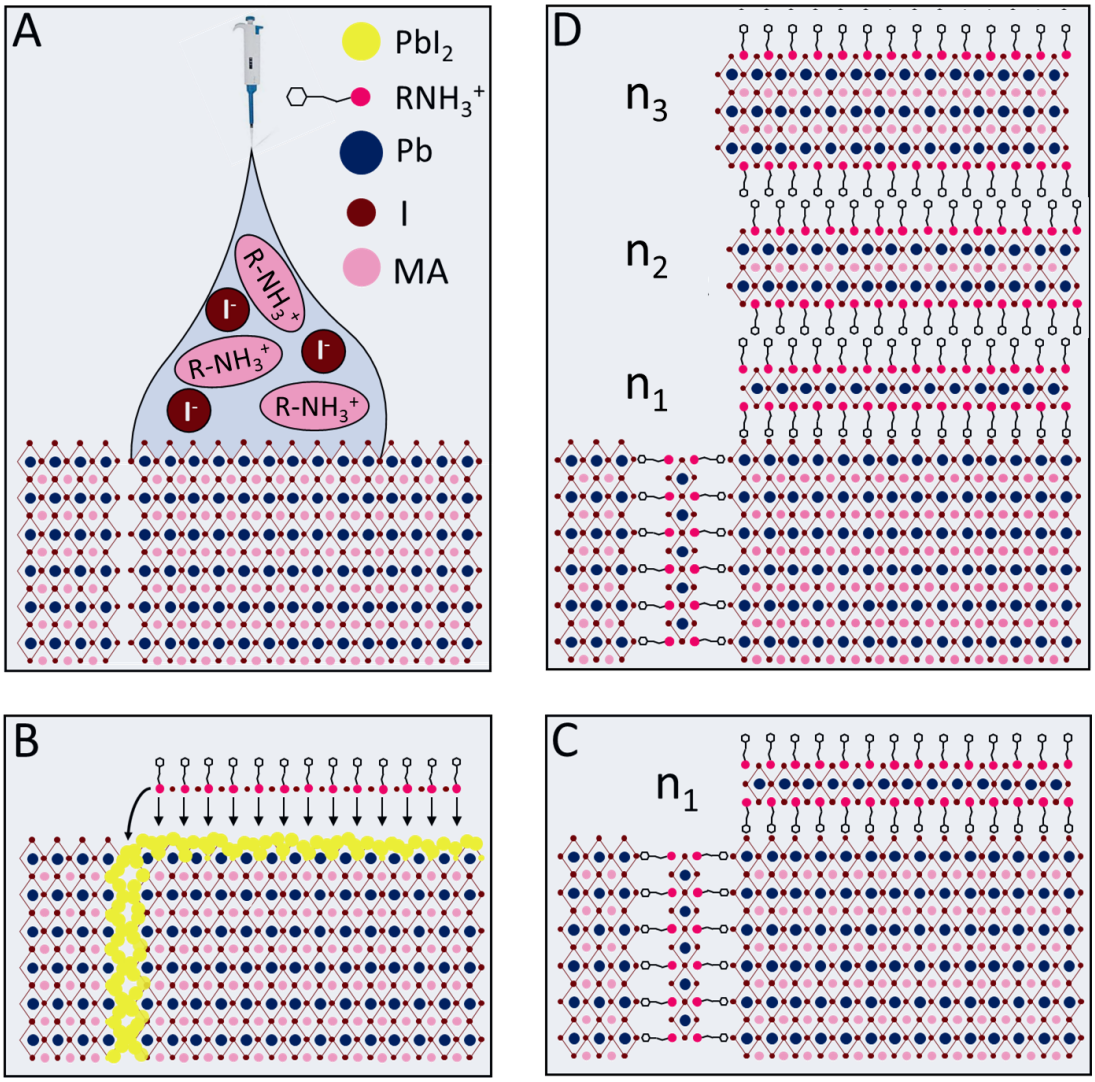

Figure 4. Proposed mechanism for R-NH_3I passivation. (a) R-NH_3I is spin-coated atop the 3D perovskite surface. (b) R-NH_3I targets PbI_2 sites. (c) R-NH_3I reacts with PbI_2 to form $(R\text{-}NH_3)_2PbI_4$ after annealing. (d) At high concentrations, excess $R\text{-}NH_3^+$ combines with MA^+ from the $MAPbI_3$ bulk to form higher order $(R\text{-}NH_3)_2MA_{n-1}Pb_nI_{3n+1}$ ($n > 1$) layered structures after annealing.

In Figure 4, We summarise the mechanism of R-NH_3I passivation in our system. Firstly, the bulky R-NH_3I reacts with PbI_2 at the 3D perovskite surface (Figure 4a and b). If [R-NH_3I] < 10 mM, the formation of pure $(R\text{-}NH_3)_2PbI_4$ at the 3D perovskite surface is favoured, with minimal disruption of the MA^+ content in the $MAPbI_3$ bulk (Figure 4c). Here, the hole injection barrier is sufficiently thin, and/or there is enough direct contact between the 3D perovskite and HTL, that charge injection can proceed efficiently. However, if [R-NH_3I] > 10 mM, a thicker $(R\text{-}NH_3)_2(MA)_{n-1}Pb_nI_{3n+1}$ ($n = 1, 2, 3\ldots$)

layer is formed (Figure 4d) due to the combination of R-NH_3^+ with intrinsic MA^+. There is some evidence that such layers stack with a *tendency* to lower n at the interface with the 3D perovskite,[36] but it is likely that the phase distribution of the RDP is highly disordered.[65] This situation then harms interfacial hole injection in three potential ways: (i) removal of intrinsic MA^+ from the 3D perovskite layer could generate trap states at the 3D/RDP interface; (ii) the disordered RDP layer containing $(R\text{-}NH_3)_2(MA)_{1\text{-}n}Pb_nI_{3n+1}$ (n = 1, 2…) could form trap states via hole funnelling; and (iii) the tunnelling yield through the RDP layer decreases exponentially with layer thickness. The 10 mM optimum concentration for PEAI found herein is in excellent agreement with the optimum PCE found elsewhere,[29,66] on $MAPbI_3$-based PSCs with a 1:1 stoichiometry. We note that the optimum concentration of PEAI would likely increase in the case of PbI_2 rich stoichiometry.[25]

Ultimately, during R-NH_3I passivation with bulky ammonium iodide salts, the passivation layer at the 3D perovskite surface undergoes a transformation from PbI_2 to $(R\text{-}NH_3)_2PbI_4$. While the presence of PbI_2 at the grain boundaries has been known to exert a limited improvement on PSC efficiency,[48–50] PbI_2 is a known proponent of degradation in devices.[67] Exchanging PbI_2 for $(R\text{-}NH_3)_2PbI_4$ therefore offers a superior passivation method given that (i) the $(R\text{-}NH_3)_2PbI_4$ layer is relatively stable and water resistant, and (ii) the charge extraction efficiency, and by extension PCE, is much enhanced.

In conclusion, we presented a comprehensive investigation of the passivation and charge transfer mechanism at 3D/RDP|HTL heterojunctions. We showed that passivation ensues via a mechanism by which R-NH_3I reacts with excess PbI_2 in the 3D perovskite film to form a layered $(R\text{-}NH_3)_2(MA)_{n\text{-}1}Pb_nI_{3n+1}$ heterostructure. We revealed that the RDP layer does not actively mediate hole transfer between the 3D perovskite and HTL layers, implying that interfacial hole injection occurs via tunnelling, regions of direct 3D|HTL contact, or a combination of both. As such, precise growth of the RDP layer is critical, with n = 1 yielding a significant improvement in interfacial hole injection across the 3D/2D|HTL interface, but n > 1 being detrimental to charge injection. We expect that proper consideration of the resulting 3D/RDP interface in these systems will aid the design of future

passivation strategies capable of further enhancing the efficiency and stability of perovskite optoelectronics.

Associated Content

Supporting Information

Transient Absorption Spectra of $MAPbI_3$ and $MAPbI_3$|PTAA; Grazing Incidence X-Ray Diffraction patterns of $MAPbI_3$ passivated with different R-NH_3I coatings; Steady-state Photoluminescence spectra of a 3D/RDP film with excitation at the air and substrate interfaces; Steady-State Photoluminescence Spectra of $MAPbI_3$ treated with R-NH_3I salts; X-Ray Diffraction patters for $MAPbI_3$ treated with different concentrations of PEAI; Steady-State Photoluminescence spectra of $MAPbI_3$ treated with different concentrations of PEAI; Absorption Spectra of 3D, 2D and 3D/RDP films; Femtosecond Transient Absorption Characterisation of 3D/RDP films; Materials and Methods.

Author Information

Corresponding Authors

Robert J E Westbrook –

Saif A Haque –

Notes

The authors declare no competing financial interest.

Acknowledgements

RW was supported by the EPSRC Centre for Doctoral Training in Advanced Characterisation of Materials (grant number EP/L015277/1). SAH acknowledges support from EPSRC (grant numbers EP/R020574/1, EP/P032591/1 and EP/R023581/1). WX is funded by the China Scholarship Council. TW thanks the University of Surrey doctoral college. TMC acknowledges EP/N026411/1. We thank James R. Durrant for supporting us with the fs-TAS measurements and the SUNRISE project for their funds (EP/P032591/1).

References

(1) nrel.gov. 2021, Best Research Cell Efficiencies https://www.nrel.gov/pv/assets/pdfs/best-research-cell-efficiencies.20200128.pdf (accessed Mar 4, 2021).

(2) Meggiolaro, D.; Motti, S. G.; Mosconi, E.; Barker, A. J.; Ball, J.; Riccardo, A.; Deschler, F.; Petrozza, A.; De Angelis, F. Iodine Chemistry Determines the Defect Tolerance of Lead-Halide Perovskites. *Energy Environ. Sci.* **2018**, *11*, 702–713.

(3) Yang, Y.; Yang, M.; Moore, D. T.; Yan, Y.; Miller, E. M.; Zhu, K.; Beard, M. C. Top and Bottom Surfaces Limit Carrier Lifetime in Lead Iodide Perovskite Films. *Nat. Energy* **2017**, *2*, 16207.

(4) Chen, P.; Bai, Y.; Wang, S.; Lyu, M.; Yun, J.; Wang, L. In Situ Growth of 2D Perovskite Capping Layer for Stable and Efficient Perovskite Solar Cells. *Adv. Funct. Mater.* **2018**, *28*, 1706923.

(5) Stolterfoht, M.; Wolff, C. M.; Márquez, J. A.; Zhang, S.; Hages, C. J.; Rothhardt, D.; Albrecht, S.; Burn, P. L.; Meredith, P.; Unold, T.; et al. Visualization and Suppression of Interfacial Recombination for High-Efficiency Large-Area Pin Perovskite Solar Cells. *Nat. Energy* **2018**, *3*, 847–854.

(6) Correa Baena, J. P.; Steier, L.; Tress, W.; Saliba, M.; Neutzner, S.; Matsui, T.; Giordano, F.; Jacobsson, T. J.; Srimath Kandada, A. R.; Zakeeruddin, S. M.; et al. Highly Efficient Planar Perovskite Solar Cells through Band Alignment Engineering. *Energy Environ. Sci.* **2015**, *8*, 2928–2934.

(7) Eames, C.; Frost, J. M.; Barnes, P. R. F.; O'Regan, B. C.; Walsh, A.; Islam, M. S. Ionic Transport in Hybrid Lead Iodide Perovskite Solar Cells. *Nat. Commun.* **2015**, *6*, 7497.

(8) Shao, Y.; Xiao, Z.; Bi, C.; Yuan, Y.; Huang, J. Origin and Elimination of Photocurrent Hysteresis by Fullerene Passivation in CH3NH3PbI3 Planar Heterojunction Solar Cells. *Nat. Commun.* **2014**, *5*, 5784–5790.

(9) Aziz, A.; Aristidou, N.; Bu, X.; Westbrook, R. J. E.; Haque, S. A.; Islam, M. S. Understanding the Enhanced Stability of Bromide Substitution in Lead Iodide Perovskites. *Chem. Mater.* **2019**, *32*, 400–409.

(10) Braly, I. L.; DeQuilletes, D. W.; Pazos-Outón, L. M.; Burke, S.; Ziffer, M. E.; Ginger, D. S.; Hillhouse, H. W. Hybrid Perovskite Films Approaching the Radiative Limit with over 90% Photoluminescence Quantum Efficiency. *Nat. Photonics* **2018**, *12*, 355–362.

(11) Noel, N. K.; Abate, A.; Stranks, S. D.; Parrott, E. S.; Burlakov, V. M.; Goriely, A.; Snaith, H. J. Enhanced Photoluminescence and Solar Cell Performance via Lewis Base Passivation of Organic-Inorganic Lead Halide Perovskites. *ACS Nano* **2014**, *8* (10), 9815–9821.

(12) Xu, G.; Nuryyeva, S.; Huang, T.; Zhao, Y.; Yang, J. L.; Zhu, J.; Wang, M.; Tan, S.; Yavuz, I.; Houk, K. N.; et al. Constructive Molecular Configurations for Surface-Defect Passivation of Perovskite Photovoltaics. *Science.* **2019**, *366*, 1509–1513.

(13) Zuo, L.; Guo, H.; Dane, W.; Jariwala, S.; Marco, N. De; Dong, S.; Deblock, R.; Ginger, D. S.; Dunn, B.; Wang, M.; et al. Polymer-Modified Halide Perovskite Films for Efficient and Stable Planar Heterojunction Solar Cells. *Sci. Adv.* **2017**, *3*, e1700106.

(14) Kim, M.; Motti, S. G.; Sorrentino, R.; Petrozza, A. Enhanced Solar Cell Stability by Hygroscopic Polymer Passivation of Metal Halide Perovskite Thin Film. *Energy Environ. Sci.* **2018**, *11*, 2609–2619.

(15) Jiang, J.; Wang, Q.; Jin, Z.; Zhang, X.; Lei, J.; Bin, H.; Zhang, Z. Polymer Doping for High-Efficiency Perovskite Solar Cells with Improved Moisture Stability. *Adv. Energy Mater.* **2018**, *8*, 1701757.

(16) Zeng, Q.; Zhang, X.; Feng, X.; Lu, S.; Chen, Z.; Yong, X.; Redfern, S. A. T.; Wei, H.; Wang, H.; Shen, H.; et al. Polymer-Passivated Inorganic Cesium Lead Mixed-Halide Perovskites for Stable and Efficient Solar Cells with High Open-Circuit Voltage over 1.3 V. *Adv. Mater.* **2018**, *30*, 1705393.

(17) Xu, W.; Hu, Q.; Bai, S.; Bao, C.; Miao, Y.; Yuan, Z.; Borzda, T.; Barker, A. J.; Tyukalova, E.; Hu, Z.; et al. Rational Molecular Passivation for High-Performance Perovskite Light-Emitting Diodes. *Nat. Photonics* **2019**, *13*, 418–424.

(18) Zheng, X.; Chen, B.; Dai, J.; Fang, Y.; Bai, Y.; Lin, Y.; Wei, H.; Zeng, X. C.; Huang, J. Defect Passivation in Hybrid Perovskite Solar Cells Using Quaternary Ammonium Halide Anions and Cations. *Nat. Energy* **2017**, *2*, 17102.

(19) Goldschmidt, V. M. Die Gesetze Der Krystallochemie. *Naturwissenschaften* **1926**, *14*, 477.

(20) Cohen, B. El; Gamliel, S.; Etgar, L. Parameters Influencing the Deposition of Methylammonium Lead Halide Iodide in Hole Conductor Free Perovskite-Based Solar Cells. *APL Mater.* **2014**, *2*, 081502.

(21) Liao, K.; Yang, J. A.; Li, C.; Li, T.; Hao, F. Off-Stoichiometric Methylammonium Iodide Passivated Large-Grain Perovskite Film in Ambient Air for Efficient Inverted Solar Cells. *ACS Appl. Mater. Interfaces* **2019**, *11*, 39882–39889.

(22) Hawash, Z.; Raga, S. R.; Son, D. Y.; Ono, L. K.; Park, N. G.; Qi, Y. Interfacial Modification of Perovskite Solar Cells Using an Ultrathin MAI Layer Leads to Enhanced Energy Level Alignment, Efficiencies, and Reproducibility. *J. Phys. Chem. Lett.* **2017**, *8*, 3947–3953.

(23) Wang, Z.; Lin, Q.; Chmiel, F. P.; Sakai, N.; Herz, L. M.; Snaith, H. J. Efficient Ambient-Air-Stable Solar Cells with 2D–3D Heterostructured Butylammonium-Caesium- Formamidinium Lead Halide Perovskites. *Nat. Energy* **2017**, *2*, 17135.

(24) Grancini, G.; Roldan-Carmona, C.; Zimmerman, I.; Mosconi, E.; Lee, X.; Martineau, D.; Narbey, S.; Oswald, F.; De Angelis, F.; Graetzel, M.; et al. One-Year Stable Perovskite Solar Cells by 2D/3D Interface Engineering. *Nat. Commun.* **2017**, *8*, 15684.

(25) Cho, Y.; Soufiani, A. M.; Yun, J. S.; Kim, J.; Lee, D. S.; Seidel, J.; Deng, X.; Green, M. A.; Huang, S.; Ho-baillie, A. W. Y. Mixed 3D–2D Passivation Treatment for Mixed-Cation Lead Mixed-Halide Perovskite Solar Cells for Higher Efficiency and Better Stability. *Adv. Energy Mater.* **2018**, *8*, 1703392.

(26) Cho, K. T.; Grancini, G.; Lee, Y.; Oveisi, E.; Ryu, J.; Almora, O.; Tschumi, M.; Schouwink, P. A.; Seo, G.; Heo, S.; et al. Selective Growth of Layered Perovskites for Stable and Efficient Photovoltaics. *Energy Environ. Sci.* **2018**, *11*, 952–959.

(27) Chen, P.; Bai, Y.; Wang, S.; Lyu, M.; Yun, J.; Wang, L. In Situ Growth of 2D Perovskite Capping Layer for Stable and Efficient Perovskite Solar Cells. *Adv. Funct. Mater.* **2018**, *28*, 1706923.

(28) Yoo, J. J.; Wieghold, S.; Sponseller, M. C.; Chua, M. R.; Bertram, S. N.; Hartono, N. T. P.; Tresback, J. S.; Hansen, E. C.; Correa-Baena, J. P.; Bulović, V.; et al. An Interface Stabilized Perovskite Solar Cell with High Stabilized Efficiency and Low Voltage Loss. *Energy Environ. Sci.* **2019**, *12*, 2192–2199.

(29) Chen, J.; Seo, J.; Park, N. Simultaneous Improvement of Photovoltaic Performance and Stability by In Situ Formation of 2D Perovskite at (FAPbI3)0.88(CsPbBr3)0.12/CuSCN Interface. *Adv. Energy Mater.* **2018**, *8*, 1702714.

(30) Liu, Y.; Akin, S.; Hinderhofer, A.; Eickemeyer, F. T.; Zhu, H.; Seo, J.; Zhang, J.; Schreiber, F.;

Zhang, H.; Zakeeruddin, S. M.; et al. Stabilization of Highly Efficient and Stable Phase-Pure FAPbI3 Perovskite Solar Cells by Molecularly Tailored 2D-Overlayers. *Angew. Chemie Int. Ed.* **2020**, *59*, 2–9.

(31) Cho, K. T.; Zhang, Y.; Orlandi, S.; Cavazzini, M.; Zimmermann, I.; Lesch, A.; Tabet, N.; Pozzi, G.; Grancini, G.; Nazeeruddin, M. K. Water-Repellent Low-Dimensional Fluorous Perovskite as Interfacial Coating for 20% Efficient Solar Cells. *Nano Lett.* **2018**, *18*, 5647–5474.

(32) Koh, T. M.; Shanmugam, V.; Guo, X.; Lim, S. S.; Filonik, O.; Herzig, E. M.; Muller-Buschbaum, P.; Swamy, V.; Chien, S. T.; Mhaisalkar, S. G.; et al. Enhancing Moisture Tolerance in Efficient Hybrid 3D/2D Perovskite Photovoltaics. *J. Mater. Chem. A* **2018**, *6*, 2122–2128.

(33) Bai, Y.; Xiao, S.; Hu, C.; Zhang, T.; Meng, X.; Lin, H.; Yang, Y.; Yang, S. Dimensional Engineering of a Graded 3D–2D Halide Perovskite Interface Enables Ultrahigh Voc Enhanced Stability in the p-i-n Photovoltaics. *Adv. Energy Mater.* **2017**, *7*, 1701038.

(34) Jung, E. H.; Joon, J. N.; Park, E. Y.; Moon, C. S.; Shin, T. J.; Yang, T.-Y.; Noh, J. H.; Seo, J. Efficient, Stable and Scalable Perovskite Solar Cells Using Poly(3-Hexylthiophene). *Nature* **2019**, *567*, 511–515.

(35) La-Placa, M. G.; Gil-Escrig, L.; Guo, D.; Palazon, F.; Savenije, T. J.; Sessolo, M.; Bolink, H. J. Vacuum-Deposited 2D/3D Perovskite Heterojunctions. *ACS Energy Lett.* **2019**, *4*, 2893–2901.

(36) Shang, Q.; Wang, Y.; Zhong, Y.; Mi, Y.; Qin, L.; Zhao, Y.; Qiu, X.; Liu, X.; Zhang, Q. Unveiling Structurally Engineered Carrier Dynamics in Hybrid Quasi- Two-Dimensional Perovskite Thin Films toward Controllable Emission. *J. Phys. Chem. Lett.* **2017**, *8*, 4431–4438.

(37) Milot, R. L.; Sutton, R. J.; Eperon, G. E.; Haghighirad, A. A.; Hardigree, J. M.; Miranda, L.; Snaith, H. J.; Johnston, M. B.; Herz, L. M. Charge-Carrier Dynamics in 2D Hybrid Metal − Halide Perovskites. *Nano Lett* **2016**, *16*, 7001–7007.

(38) Motti, S. G.; Crothers, T.; Yang, R.; Cao, Y.; Li, R.; Johnston, M. B.; Wang, J.; Herz, L. M. Heterogeneous Photon Recycling and Charge Diffusion Enhance Charge Transport in Quasi-2D Lead-Halide Perovskite Films. *Nano Lett.* **2019**, *19*, 3953–3960.

(39) Krishna, A.; Gottis, S.; Nazeeruddin, M. K.; Sauvage, F. Mixed Dimensional 2D/3D Hybrid Perovskite Absorbers: The Future of Perovskite Solar Cells? *Adv. Funct. Mater.* **2019**, *29*, 1806482.

(40) Bouduban, M. E. F.; Queloz, V. I. E.; Caselli, V. M.; Cho, K. T.; Kirmani, A. R.; Paek, S.; Roldan-Carmona, C.; Richter, L. J.; Moser, J. E.; Savenije, T. J.; et al. Crystal Orientation Drives the Interface Physics at Two/Three-Dimensional Hybrid Perovskites. *J. Phys. Chem. Lett.* **2019**, *10*, 5713–5720.

(41) Sutanto, A. A.; Drigo, N.; Queloz, V. I. E.; Garcia-Benito, I.; Kirmani, A. R.; Richter, L. J.; Schouwink, P. A.; Cho, K. T.; Paek, S.; Nazeeruddin, M. K.; et al. Dynamical Evolution of the 2D/3D Interface: A Hidden Driver behind Perovskite Solar Cell Instability. *J. Mater. Chem. A* **2020**, *8*, 2343–2348.

(42) Teale, S.; Proppe, A. H.; Jung, E. H.; Johnston, A.; Parmar, D. H.; Chen, B.; Hou, Y.; Kelley, S. O.; Sargent, E. H. Dimensional Mixing Increases the Efficiency of 2D/3D Perovskite Solar Cells. *J. Phys. Chem. Lett.* **2020**, *11*, 5115–5119.

(43) Proppe, A. H.; Wei, M.; Chen, B.; Quintero-Bermudez, R.; Kelley, S. O.; Sargent, E. H. Photochemically Cross-Linked Quantum Well Ligands for 2D/3D Perovskite Photovoltaics with Improved Photovoltage and Stability. *J. Am. Chem. Soc.* **2019**, *141*, 14180–14189.

(44) Kanatzidis, M. G. 2D Homologous Perovskites as Light-Absorbing Materials for Solar Cell Applications. *J. Am. Chem. Soc.* **2015**, *137*, 7843–7850.

(45) Jeon, N. J.; Noh, J. H.; Kim, Y. C.; Yang, W. S.; Ryu, S.; Seok, S. Il. Solvent Engineering for High-Performance Inorganic – Organic Hybrid Perovskite Solar Cells. *Nat. Mater.* **2014**, *13*, 897–903.

(46) Westbrook, R. J. E.; Sanchez-Molina, I.; Marin-Beloqui, J. M.; Bronstein, H.; Haque, S. A. Effect of Interfacial Energetics on Charge Transfer from Lead Halide Perovskite to Organic Hole Conductors. *J. Phys. Chem. C* **2018**, *122*, 1326–1332.

(47) Klein, J. R.; Scholz, M.; Oum, K.; Lenzer, T. Intramolecular and Interfacial Dynamics of Triarylamine-Based Hole Transport Materials. *Photochem. Photobiol. Sci.* **2018**, *17*, 722–733.

(48) Du, T.; Burgess, C. H.; Kim, J.; Zhang, J.; Durrant, R.; Mclachlan, M. A. Formation, Location and Beneficial Role of PbI2 in Lead Halide Perovskite Solar Cells. *Sustain. Energy Fuels* **2017**, *1*, 119–126.

(49) Chen, Q.; Zhou, H.; Song, T. Bin; Luo, S.; Hong, Z.; Duan, H. S.; Dou, L.; Liu, Y.; Yang, Y. Controllable Self-Induced Passivation of Hybrid Lead Iodide Perovskites toward High Performance Solar Cells. *Nano Lett.* **2014**, *14*, 4158–4163.

(50) Kim, Y. C.; Jeon, N. J.; Noh, J. H.; Yang, W. S.; Seo, J.; Yun, J. S.; Ho-Baillie, A.; Huang, S.; Green, M. A.; Seidel, J.; et al. Beneficial Effects of PbI2 Incorporated in Organo-Lead Halide Perovskite Solar Cells. *Adv. Energy Mater.* **2016**, *6*, 1502104.

(51) Rashad, M. M.; Elseman, A. M.; Hassan, A. M. Facile Synthesis, Characterization and Structural Evolution of Nanorods Single-Crystalline (C4H9NH3)2PbI2X2 Mixed Halide Organometal Perovskite for Solar Cell Application. *Optik.* **2016**, *127*, 9775–9787.

(52) Jones, T. W.; Osherov, A.; Alsari, M.; Sponseller, M.; Duck, B. C.; Jung, Y. K.; Settens, C.; Niroui, F.; Brenes, R.; Stan, C. V.; et al. Lattice Strain Causes Non-Radiative Losses in Halide Perovskites. *Energy Environ. Sci.* **2019**, *12*, 596–606.

(53) Kamminga, M. E.; Fang, H. H.; Filip, M. R.; Giustino, F.; Baas, J.; Blake, G. R.; Loi, M. A.; Palstra, T. T. M. Confinement Effects in Low-Dimensional Lead Iodide Perovskite Hybrids. *Chem. Mater.* **2016**, *28*, 4554–4562.

(54) Smith, M. D.; Connor, B. A.; Karunadasa, H. I. Tuning the Luminescence of Layered Halide Perovskites. *Chem. Rev.* **2019**, *119*, 3104–3139.

(55) Stoumpos, C. C.; Cao, D. H.; Clark, D. J.; Young, J.; Rondinelli, J. M.; Jang, J. I.; Hupp, J. T.; Kanatzidis, M. G. Ruddlesden−Popper Hybrid Lead Iodide Perovskite 2D Homologous Semiconductors. *Chem. Mater.* **2016**, *28*, 2852–2867.

(56) Shi, D.; Adinolfi, V.; Comin, R.; Yuan, M.; Alarousu, E.; Buin, A.; Chen, Y.; Hoogland, S.; Rothenberger, A.; Katsiev, K.; et al. Low Trap-State Density and Long Carrier Diffusion in Organolead Trihalide Perovskite Single Crystals. *Science.* **2015**, *347*, 519–522.

(57) Wen, X.; Sheng, R.; Ho-baillie, A. W. Y.; Benda, A.; Woo, S.; Ma, Q.; Huang, S.; Green, M. A. Morphology and Carrier Extraction Study of Organic − Inorganic Metal Halide Perovskite by One- and Two-Photon Fluorescence Microscopy. *J. Phys. Chem. Lett.* **2014**, *5*, 3849.

(58) Silver, S.; Yin, J.; Li, H.; Brédas, J. L.; Kahn, A. Characterization of the Valence and Conduction Band Levels of n = 1 2D Perovskites: A Combined Experimental and Theoretical Investigation. *Adv. Energy Mater.* **2018**, *8*, 1703468.

(59) Cho, K. T.; Grancini, G.; Lee, Y.; Oveisi, E.; Ryu, J.; Almora, O.; Tschumi, M.; Schouwink, P. A.;

Seo, G.; Heo, S.; et al. Selective Growth of Layered Perovskites for Stable and Efficient Photovoltaics. *Energy Environ. Sci.* **2018**, *11*, 952–959.

(60) Cao, D. H.; Stoumpos, C. C.; Farha, O. .; Hupp, J. T.; Kanatzidis, M. G. 2D Homologous Perovskites as Light-Absorbing Materials for Solar Cell Applications. *J. Am. Chem. Soc.* **2015**, *137*, 7843–7850.

(61) Xing, G.; Mathews, N.; Lim, S. S.; Lam, Y. M.; Mhaisalkar, S.; Sum, T. C. Long-Range Balanced Electron- and Hole-Transport Lengths in Organic-Inorganic CH3NH3PbI3. *Science.* **2013**, *342*, 344–348.

(62) Manser, J. S.; Kamat, P. V. Band Filling with Free Charge Carriers in Organometal Halide Perovskites. *Nat. Photonics* **2014**, *8*, 737–743.

(63) Stamplecoskie, K. G.; Manser, J. S.; Kamat, P. V. Dual Nature of the Excited State in Organic-Inorganic Lead Halide Perovskites. *Energy Environ. Sci.* **2015**, *8*, 208–215.

(64) Marchioro, A.; Teuscher, J.; Friedrich, D.; Kunst, M.; van de Krol, R.; Moehl, T.; Gratzel, M.; Moser, J.-E. Unravelling the Mechanism of Photoinduced Charge Transfer Processes in Lead Iodide Perovskite Solar Cells. *Nat Phot.* **2014**, *8*, 250–255.

(65) Xu, Y.; Wang, M.; Lei, Y.; Ci, Z.; Jin, Z. Crystallization Kinetics in 2D Perovskite Solar Cells. *Adv. Energy Mater.* **2020**, 2002558.

(66) Bu, X.; Westbrook, R. J. E.; Lanzetta, L.; Ding, D.; Chotchuangchutchaval, T.; Aristidou, N.; Haque, S. A. Surface Passivation of Perovskite Films via Iodide Salt Coatings for Enhanced Stability of Organic Lead Halide Perovskite Solar Cells. *Sol. RRL* **2019**, *3*, 1800282.

(67) Tumen-Ulzii, G.; Qin, C.; Klotz, D.; Leyden, M. R.; Wang, P.; Auffray, M.; Fujihara, T.; Matsushima, T.; Lee, J. W.; Lee, S. J.; et al. Detrimental Effect of Unreacted PbI2 on the Long-Term Stability of Perovskite Solar Cells. *Adv. Mater.* **2020**, *32*, 1905035.